



CHORUS

This is the accepted manuscript made available via CHORUS. The article has been published as:

Band edge evolution of transparent $\text{ZnM}_{2}^{\text{III}}\text{O}_{4}$ ($\text{M}^{\text{III}} = \text{Co, Rh, Ir}$) spinels

Matthew J. Wahila, Zachary W. Lebens-Higgins, Adam J. Jackson, David O. Scanlon, Tien-Lin Lee, Jiaye Zhang, Kelvin H. L. Zhang, and Louis F. J. Piper

Phys. Rev. B **100**, 085126 — Published 15 August 2019

DOI: [10.1103/PhysRevB.100.085126](https://doi.org/10.1103/PhysRevB.100.085126)

Band Edge Evolution of Transparent $\text{ZnM}_2^{\text{III}}\text{O}_4$ ($\text{M}^{\text{III}} = \text{Co}, \text{Rh}, \text{Ir}$) Spinels

Matthew J. Wahila,¹ Zachary W. Lebens-Higgins,¹ Adam J. Jackson,^{2,3} David O. Scanlon,^{2,3} Tien-Lin Lee,⁴ Jiaye Zhang,⁵ Kelvin H. L. Zhang,^{5,6} and Louis F. J. Piper^{1,7}

¹*Department of Physics, Applied Physics and Astronomy,
Binghamton University, Binghamton, New York 13902, USA*

²*Department of Chemistry, University College London, London WC1H 0AJ, UK*

³*Thomas Young Centre, University College London, London WC1E 6BT, UK*

⁴*Diamond Light Source Ltd., Harwell Science and Innovation Campus, Didcot, OX11 0DE, UK*

⁵*State Key Laboratory of Physical Chemistry of Solid Surfaces,*

College of Chemistry and Chemical Engineering, Xiamen University, Xiamen 361005, China

⁶*Department of Materials Science & Metallurgy, University of Cambridge, Cambridge CB3 0FS, UK*

⁷*Material Science & Engineering, Binghamton University, Binghamton, New York 13902, USA**

$\text{ZnM}_2^{\text{III}}\text{O}_4$ ($\text{M}^{\text{III}} = \text{Co}, \text{Rh}, \text{Ir}$) spinels have been recently identified as promising p-type semiconductors for transparent electronics. However, discrepancies exist in the literature regarding their fundamental optoelectronic properties. In this study, the electronic structures of these spinels are directly investigated using soft/hard x-ray photoelectron and x-ray absorption spectroscopies in conjunction with density functional theory calculations. In contrast to previous results, ZnCo_2O_4 is found to have a small electronic band gap with forbidden optical transitions between the true band edges, allowing for both bipolar doping and high optical transparency. Furthermore, increased $d-d$ splitting combined with a concomitant lowering of Zn s/p conduction states is found to result in a $\text{ZCO} < \text{ZRO} \approx \text{ZIO}$ band gap trend, finally resolving long-standing discrepancies in the literature.

I. INTRODUCTION

Transparent oxide semiconductors (TOS) combining tunable electrical conductivity and optical transparency hold great promise for a wide range of applications, including solar cells, flat-panel displays, UV photodetectors, and transparent transistors.¹⁻⁴ Most TOS to date are n-type semiconductors composed of post-transition metal oxides, e.g., In_2O_3 , Ga_2O_3 , SnO_2 , and ZnO , as their metal ns -derived conduction states give rise to a dispersive conduction band minima with low electron effective mass. In contrast, p-type conduction in these oxides is typically poor due to their localized O $2p$ -derived valence band maxima. However, hybridization between the O $2p$ and metal orbitals has been shown to improve hole dispersion, as in some Cu^+ -based delafossites, Cr^{3+} -based oxides, and post-transition metal oxides with a filled lone pair state (ns^2).⁵⁻¹⁰ Unfortunately, some common theoretical methods are known to be unreliable when predicting properties of mixed oxides with potentially complex local interactions,¹¹ hampering computation-led materials genome initiatives that exist to accelerate the discovery of these materials.

Herein we illustrate the benefits of using careful experimental studies to guide computational efforts by explaining the optoelectronic properties of $\text{ZnM}_2^{\text{III}}\text{O}_4$ ($\text{M}^{\text{III}} = \text{Co}, \text{Rh}, \text{Ir}$) spinels, which have been identified as promising p-type TOS by recent studies.¹²⁻¹⁵ Some studies have even indicated that transparent ZnCo_2O_4 may be well-suited for complementary metal-oxide-semiconductor (CMOS) electronics applications,¹⁶ as it is amenable to bipolar doping with both n- or p-type possible through control of oxygen content.¹⁷ This bipolar dopability indicates that ZnCo_2O_4 , and likely ZnRh_2O_4 and ZnIr_2O_4 as well, must possess small elec-

tronic band gaps despite their high optical transparency (i.e., wide optical band gaps).¹⁸⁻²¹ In addition, it has been shown that the local O-Rh-O octahedral network in ZnRh_2O_4 can be preserved in an amorphous phase, allowing for good hole conduction pathways without high film crystallinity.^{22,23} This is in stark contrast to other p-type TOS, such as CuAlO_2 delafossite, where disorder disrupts the linear O-Cu-O coordination and greatly impedes hole conduction.⁵

In spite of their potential promise, many discrepancies exist in the literature regarding the fundamental properties of these $\text{ZnM}_2^{\text{III}}\text{O}_4$ spinels. There is a clear lack of consensus regarding band gap magnitudes, with some studies suggesting a decrease in the band gap from Co to Rh and others an increase from Co to Rh.^{13,17,24,25} Optical studies have reported band gaps of 2.63 - 2.8 eV for ZnCo_2O_4 ,^{17,26} a much smaller 2 eV optical gap for ZnRh_2O_4 ,^{13,27} and a range of values between 2.1 - 2.7 eV for ZnIr_2O_4 .¹⁴ Meanwhile, a more wide-ranging study by Dekkers et al. reports drastically different values of 2.26 eV, 2.74 eV, and 2.97 eV for ZnCo_2O_4 , ZnRh_2O_4 , and ZnIr_2O_4 , respectively.²⁸

Theoretical studies have attempted to resolve these conflicting results with mixed success. As many common Density Functional Theory (DFT) methods are known to underestimate the band gaps of metal oxides, some have attempted to improve accuracy through the use of more complex hybrid functionals.^{25,29,30} However, others have questioned the accuracy of these methods regarding mixed cation oxides, reporting that calculations using the PBE⁰ hybrid functional resulted in the Co $d-d$ splitting of Co-doped ZnO being overestimated by as much as 300% compared to experiment.¹¹ It is clear that a thorough experimental study is needed to understand these spinels and resolve the discrepancies in the literature.

In this study, a set of high quality ZnCo_2O_4 (ZCO), ZnRh_2O_4 (ZRO), and ZnIr_2O_4 (ZIO) epitaxial thin films are investigated using synchrotron-based x-ray spectroscopy techniques to discern the true band edge structures. These results are then combined with DFT PBEsol calculations^{31–37} to confirm orbital compositions of the band edges and explain the observed optoelectronic trends. The results reveal that these $\text{ZnM}_2^{\text{III}}\text{O}_4$ spinels possess smaller electronic gaps than previously measured by optical techniques, explaining their bipolar doping potential. In addition, overlap of the Zn s - and M^{III} d -orbitals in ZnIr_2O_4 due to shrinking O $2p$ - Zn $4s/p$ splitting is responsible for the confusion in the literature surrounding the band gap evolution.

II. EXPERIMENTAL METHODS

$\text{ZnM}_2^{\text{III}}\text{O}_4$ ($M^{\text{III}} = \text{Co}, \text{Rh}, \text{Ir}$) thin films possessing the spinel structure, shown in Figure 1 (a), were fabricated via pulsed laser deposition using a 248 nm KrF excimer laser with an energy density of $1.0 \text{ J} \cdot \text{cm}^{-2}$ and repetition rate of 5 Hz. The substrate temperature for all films was kept at $475 \text{ }^\circ\text{C}$ with an oxygen partial pressure of 150 mTorr for ZCO/ZRO, and 30 mTorr for ZIO. Higher oxygen partial pressures were found to give higher conductivities, while both lower and higher substrate temperatures of $375 \text{ }^\circ\text{C}$ and $550 \text{ }^\circ\text{C}$ were found to lead to the growth of a ZnO second phase. The ZCO films were grown epitaxially on $5 \times 5 \text{ mm MgAl}_2\text{O}_4(001)$ substrates, while ZRO and ZIO films were grown epitaxially on $\text{MgO}(001)$, as it is difficult to grow these films on MgAl_2O_4 due to a large lattice mismatch.

Shown in Figure 1 (b) - (d), these growth parameters resulted in crystalline, epitaxial thin films around 25 nm in thickness, as confirmed by reflection high-energy electron diffraction (RHEED), x-ray diffraction (XRD), and reciprocal space mapping (RSM). Our epitaxial ZCO is found to have in-plane and out-of-plane lattice dimensions of 8.08 \AA and 8.23 \AA , respectively, compared 8.108 \AA expected for bulk from literature. Our epitaxial ZRO has in-plane and out-of-plane lattice dimensions of 8.424 \AA and 8.730 \AA , respectively, compared to 8.510 \AA expected for bulk from literature. And our epitaxial ZIO has in-plane and out-of-plane lattice dimensions of 8.445 \AA and 8.709 \AA , respectively.

Ultraviolet-Visible (UV-Vis) transmittance spectra were measured on the films and substrate references. Optical absorption coefficients were then calculated from the spectra after subtracting out any contributions from the substrates using the thin film approximation, $T \approx (1 - R)^2 e^{-\alpha d}$, where T is the transmittance, R is the reflectance, and d is the film thickness.

Hard x-ray photoelectron spectroscopy (HAXPES) measurements were performed with a $\sim 6 \text{ keV}$ photon energy at the I09 Surface and Interface Structural Analysis beamline of the Diamond Light Source (DLS) in Oxfordshire, UK. HAXPES spectra were energy-resolved

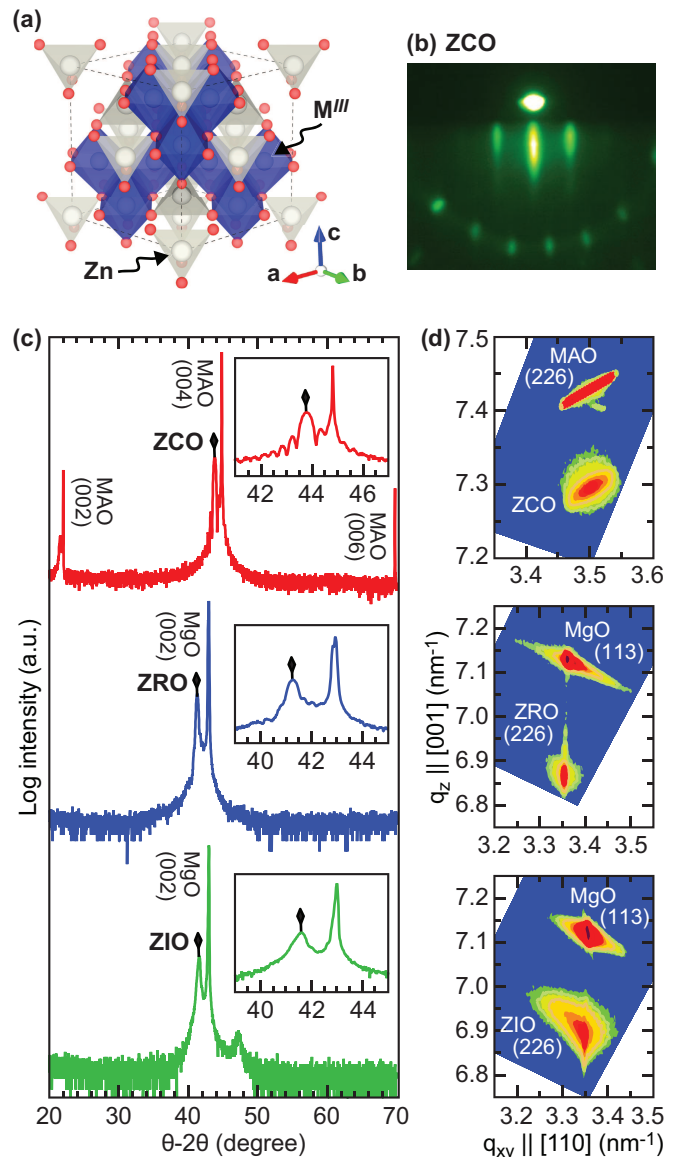


FIG. 1. (a) The spinel structure of $\text{ZnM}_2^{\text{III}}\text{O}_4$ where the M^{III} cations (Co, Rh, or Ir) occupy octahedral sites (blue) and Zn occupy tetrahedral sites (gray). (b) Reflection high-energy electron diffraction (RHEED) image taken on a ZCO film. (c) Out-of-plane θ - 2θ x-ray diffraction (XRD) for the ZCO, ZRO, and ZIO films. (d) Reciprocal space maps (RSM) for ZCO around the substrate MAO(226) reflection and for ZRO/ZIO around the substrate MgO(113) reflection.

and measured using a VG Scienta EW4000 high-energy electron-energy analyzer with a 30° acceptance angle. The HAXPES photon beam was monochromated using a channel cut Si(004) crystal followed by a Si(111) double-crystal monochromator, resulting in an overall energy resolution of $< 250 \text{ meV}$.^{38–40}

X-ray absorption spectroscopy (XAS) was performed at beamline I09, and also at beamlines 6 and 8 of the Advanced Light Source in Berkeley, CA. All XAS spectra were taken in total electron yield (TEY) mode, with

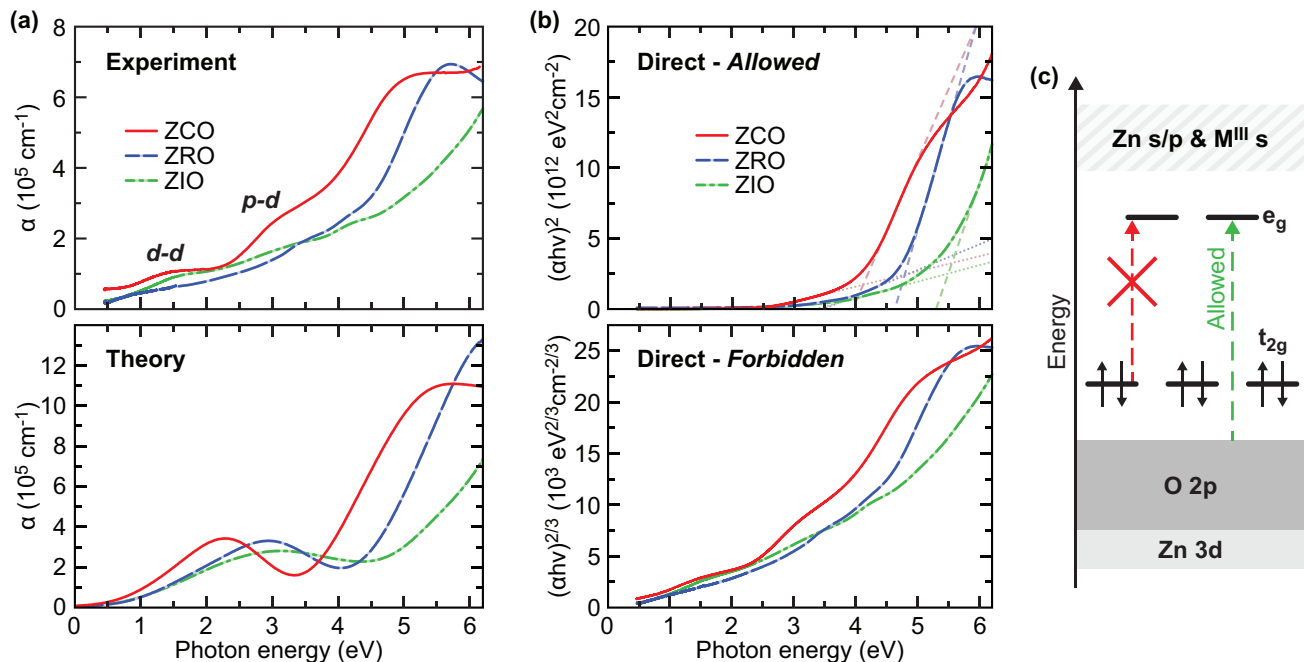


FIG. 2. (a) Optical absorption coefficients of ZCO, ZRO, and ZIO derived from (top) optical transmittance/reflectance measurements and (bottom) atomistic calculations. (b) Tauc plots emphasizing (top) direct allowed transitions and (bottom) direct forbidden transitions. Fit lines for the main optical absorption edge (dashed lines) and weaker $p-d$ associated transitions (dotted lines) are given. (c) Proposed schematic of the near E_F band configuration for $\text{ZnM}_2^{\text{III}}\text{O}_4$ spinels.

an effective resolution of ~ 200 meV. The absorption spectra were normalized to the current from a reference Au-coated mesh in the path of the incident photon beam. Energy calibration was performed using the first- and second-order diffraction Ti $L_{3,2}$ -edge and O K-edge absorption features of a rutile TiO_2 reference.

Density-functional theory (DFT) calculations were performed using the Vienna Ab Initio Simulation Package (VASP)³¹ with projector augmented-wave pseudopotential.^{32,33} A 500 eV cutoff plane-wave basis set was employed for electronic structure calculations using the PBEsol exchange-correlation functional.³⁴ The initial cubic structure for ZnCo_2O_4 (Fd-3m space group) was drawn from the Materials Project database.^{35,36} After convergence testing of the Brillouin-zone sampling for ZnCo_2O_4 , a $4 \times 4 \times 4$ Γ -centered \mathbf{k} -point mesh was used to optimize the lattice parameters and atomic positions of ZnCo_2O_4 and derived cells of ZnRh_2O_4 and ZnIr_2O_4 , reducing forces to less than 10^{-3} eV/Å. Force/energy evaluations used an energy convergence criterion of 10^{-6} eV with 0.1 eV Gaussian broadening.

Density of states (DOS) calculations were performed using the optimized structures with stricter energy convergence (10^{-7} eV between final steps), denser Brillouin-zone sampling ($6 \times 6 \times 6$ Γ -centered mesh), and increased Gaussian broadening (0.2 eV). Band structures were calculated non-self-consistently using the charge density data computed during DOS calculations. Optical absorption coefficients were computed at the same geometry using a $14 \times 14 \times 14$ \mathbf{k} -point mesh and integrating with the

Blöchl-corrected tetrahedron method.³⁷ The frequency-dependent dielectric matrix was computed within VASP by summation over empty states, obtaining the real part by a Kramers-Kronig transformation. This was then converted to absorption via the extinction coefficient.

III. RESULTS AND DISCUSSION

Figure 2 (a) shows the photon energy-dependent absorption coefficients derived from Ultraviolet-Visible (UV-Vis) transmittance spectra, as well as predicted from theoretical calculations. Qualitatively, the general shapes of the measured and predicted absorption edges agree quite well. Shown in Fig. 2 (b), band gaps can be quantitatively determined from absorption spectra using Tauc analysis, where $(\alpha h\nu)^{1/r}$ is plotted versus $h\nu$ using an r value corresponding to the type of optical transition occurring between the band edges.^{41,42} After fitting a line to the predominantly linear region of this Tauc plot, the x-intercept of said line provides an approximate value for the onset of optical absorption (i.e., the band gap), provided there is negligible background signal at photon energies below the absorption onset.

Assuming that the band gap is direct and that optical transitions are allowed ($r = 1/2$), as in the top of Fig. 2 (b), the strongest absorption onsets (dashed lines) are found to occur around 4.1, 4.7, and 5.5 eV for ZCO, ZRO, and ZIO, respectively, when taking into account the background from the weaker absorptions at lower en-

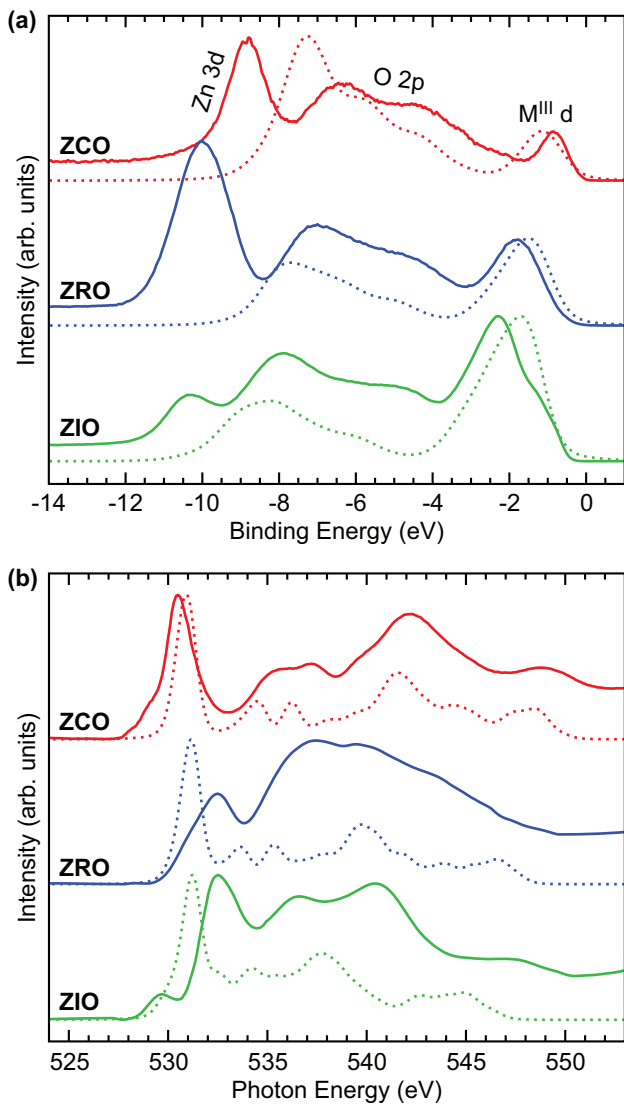


FIG. 3. (a) HAXPES (solid) and DFT PBEsol total density of states (dotted) of the ZCO, ZRO, and ZIO valence band region. (b) XAS oxygen K-edge (solid) and DFT PBEsol oxygen 2p partial density of states (dotted) of the ZCO, ZRO, and ZIO conduction band region.

ergies. These values are all far too large to correspond to band gaps previously reported in the literature.²⁸ Fitting a line to the weaker optical absorptions (dotted lines) provides a slightly different band gap order of $ZCO < ZRO \approx ZIO$, with energetic onsets of 2.5, 3.5, and 3.3 eV for ZCO, ZRO, and ZIO, respectively. These values are much closer in magnitude to some previously reported values for the optical band gaps.^{17,26,28} However, a Tauc plot where $r = 1/2$ is likely not the best method for investigating the band gaps of these spinels, as optical transitions between the band edges would be forbidden if the band edges are truly M^{III} d -orbital in origin as expected.

Due to the octahedral ligand coordination of the M^{III} cation in the spinel structure, the M^{III} nd^6 orbitals will

split into three t_{2g} and two e_g states, as depicted in Fig. 2 (c). In this configuration, the lower energy (t_{2g}) states will be completely filled while the higher (e_g) states will be completely empty.^{28,43} This $d-d$ splitting is typically on the order of $\sim 2 - 3$ eV for metal oxides with octahedral coordination,^{11,43,44} while the O 2p - Zn 4s/p splitting is typically larger, at ~ 3.4 eV for ZnO.¹¹ As such, it is highly likely that M^{III} d -orbital states compose one if not both of the band edges in these spinels.

As ligand field ($d-d$) splitting typically increases with atomic number, it is not unreasonable to expect the band gaps of these spinels to increase in magnitude from Co to Rh to Ir.¹³ While some previous experimental studies do not support this conclusion, these investigations are complicated by the fact that optical transitions between t_{2g} and e_g states do not represent a change in parity and are thus forbidden according to the Laporte rule. This makes the $d-d$ splitting in these spinels difficult to investigate using optical techniques alone, as the optical absorption due to transitions between the band edges should be incredibly weak.^{23,45}

Treating these spinels as direct band gap materials but with *forbidden* band edge transitions ($r = 3/2$), as in the bottom of Fig. 2 (b), reveals a multitude of weak yet distinct absorption onsets extending down to 2 eV or below. In this case, the background at low energies is clearly non-negligible and must be properly accounted for in order to determine the band gaps with any accuracy.⁴⁶ Unfortunately, it is a non-trivial and rather subjective process to disentangle the true band edge absorption from all of the various effects potentially contributing to the background, such as wavelength dependent reflections, scattering processes not accounted for by the reference standard, or absorption from ion vacancies or other defects. However, even without accurate numerical values for the band gaps, this analysis clearly indicates that although the majority of the optical absorption occurs above ~ 3 eV, the electronic band gaps of these spinels must be smaller.

Figure 3 shows the valence and conduction band spectra for ZCO, ZRO, and ZIO as measured by multiple x-ray spectroscopy techniques, as well as calculated using DFT. It must be noted that the ZRO appears to have some ZnO-like spectral contamination potentially caused by a zinc-rich surface layer or segregated crystallites, resulting in an over-representation of Zn-related states in the experimental spectra.

Combining both high-resolution hard x-ray photoelectron spectroscopy (HAXPES)³⁸⁻⁴⁰ and x-ray absorption spectroscopy (XAS) provides crucial insight into the true evolution of both band edge. In ZCO, the sharp Co 3d t_{2g} and e_g peaks are found to make up the band edges, with a small $d-d$ splitting. In ZRO, the Rh 4d t_{2g} and e_g peaks show greater $d-d$ splitting than the Co 3d, and they also appear significantly broadened in comparison. And in ZIO, the $d-d$ peak splitting appears by far the largest, however, additional features/shoulders are present on both band edges that cannot be assigned pure Ir 5d character. These band edge changes result in

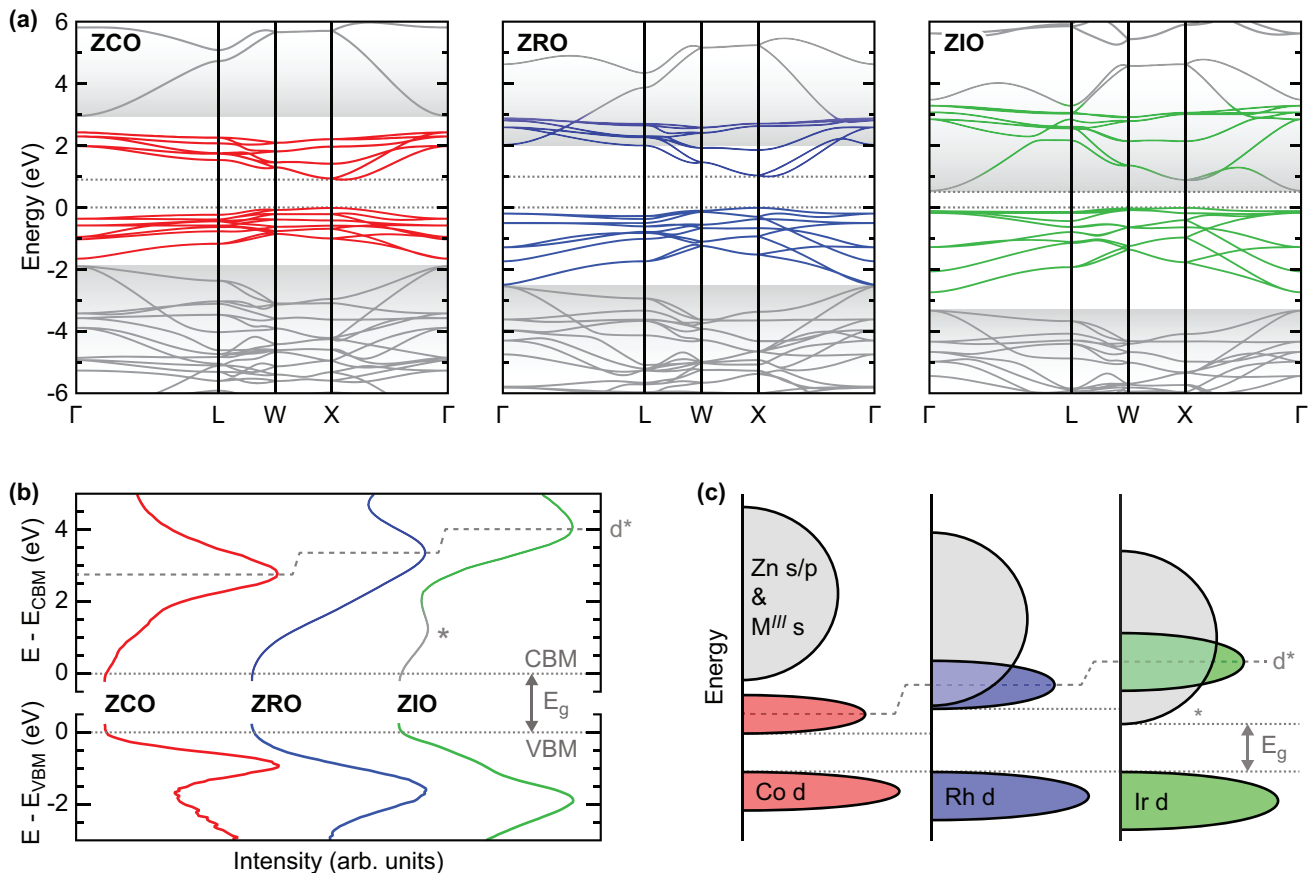


FIG. 4. (a) DFT calculated band diagrams for ZCO, ZRO, and ZIO. The $d-d$ split states (colored lines) and s/p -derived states (shaded background) are denoted. (b) Experimentally measured band edges of ZCO, ZRO, and ZIO. (c) Diagram of the proposed band edge evolution from ZCO to ZRO to ZIO. Additional states extending below the main Ir $5d$ -derived conduction band states are denoted (*).

an electronic band gap order of $\text{ZCO} < \text{ZRO} \approx \text{ZIO}$ despite the apparently larger $d-d$ splitting of ZIO relative to ZRO, in agreement with some theoretical studies.²⁵

While several theoretical studies reported in the literature have attempted to simulate the electronic structures of these ZnM_2O_4 spinels,^{25,26,29,30} a large discrepancy exists regarding the magnitudes of predicted band gaps. In general, DFT calculations result in small band gaps (e.g., 0.57, 0.80, and 0.48 eV for ZnCo_2O_4 ,²⁵ ZnRh_2O_4 , and ZnIr_2O_4 , respectively), while the hybrid exchange-correlation functional HSE06²⁵ and GW calculations³⁰ yield significantly large band gap values (e.g., 3.86, 2.87, and 2.47 eV for ZnCo_2O_4 , ZnRh_2O_4 , and ZnIr_2O_4 , respectively). In this study, comparison of our theoretical results with both the optical absorption spectra in Fig. 2 and the experimental density of states in Fig. 3, suggests that our DFT PBEsol calculations can be used to provide valuable insight into the band edge evolution.

Although the DFT shown in Fig. 3 underestimates the energetic position of the Zn $3d$ semi-core level and the band gap magnitudes, which are both well documented issues with some forms of DFT,^{11,21,47} the rest of the observed spectral features are fairly well reproduced. The

calculated spectra show a clear increase in the $d-d$ splitting from ZCO to ZRO to ZIO despite the incorrect overall magnitude, in agreement with the experimental spectra and with previous studies.^{25,28,30} The calculated spectra also reproduce the Rh $4d$ broadening, as well as the additional features/shoulders on the Ir $5d$ peaks, which are a result of greater overlap and hybridization between the unoccupied $M^{III} e_g$ and the Zn s/p and $M^{III} s$ -orbital conduction states.

Figure 4 summarizes the band edge evolution of the $\text{ZnM}_2^{III}\text{O}_4$ series as observed in this study. Fig. 4 (a) displays the full DFT calculated band diagrams for the series, clearly showing the expected interaction between the different bands. Fig. 4 (b) then shows the experimentally observed band edges, which agree well with the predicted band edge evolution. While the band edges of ZnCo_2O_4 are both composed of sharp Co $3d$ states fairly well separated from the Zn s/p , O $2p$ and Co s -related states, the band edges in ZnRh_2O_4 and ZnIr_2O_4 show far more interaction and overlap. This results in the observed $\text{ZCO} < \text{ZRO} \approx \text{ZIO}$ band gap trend and increasing band edge dispersion, which readily explains the better p-type conduction in ZRO and ZIO. This is in

agreement with a previous theoretical study which suggested the CBM of ZIO might be composed of mixed Ir s and Zn s states due to a lowering of these conduction states to below the Ir $5d$.²⁵

A simplified diagram of the observed band edge evolution is given in Fig. 4 (c). While the $d - d$ splitting is found to progressively increase from Co to Ir, the Zn $s - p$ and $M^{III} s$ conduction band states simultaneously lower in energy. This results in a conduction band edge of mainly $M^{III} d$ character in ZCO; mixed $M^{III} d$, $M^{III} s$, and Zn s/p character in ZRO; and mainly $M^{III} s$ and Zn s/p character in ZIO. This model resolves the conflicting results of previous studies by allowing for both the $d - d$ splitting to increase with increasing atomic number as expected, and the electronic band gaps to progress in the order $ZCO < ZRO \approx ZIO$.

IV. CONCLUSIONS

These findings explain the observation of both n- and p-type conduction in $ZnCo_2O_4$.¹⁷ A small electronic band gap with forbidden optical transitions between the true band edges allows for both the observed doping capabilities and the high optical transparency, similar to some other transparent metal oxides like crystalline SnO or $CuInO_2$.^{8,48,49} Furthermore, the increased conductivity of crystalline $ZnRh_2O_4$ and $ZnIr_2O_4$ relative to $ZnCo_2O_4$ ³⁰ is explained by the observed increase in hybridization at the band edges for these M^{III} cations. This conduction band edge hybridization suggests that n-type doping may also be possible in ZIO or even ZRO despite the slightly larger band gaps, provided their elec-

tron affinities remain large enough.

These results highlight the need for experimental confirmation of predicted electronic structures, especially when considering transparent mixed oxide systems such as these $ZnM_2^{III}O_4$ spinels. While certain methodologies may correctly predict the $M^{III} d - d$ splitting or the O $2p$ and Zn s/p splitting, correctly reproducing all vital aspects of the spectra would likely require far more involved calculations with explicit on-site corrections for each cation.⁴⁷ And such corrections must still be informed by prior experimental results to have any real meaning, leading to a necessity for thorough experimental studies on these mixed oxide systems.

V. ACKNOWLEDGMENTS

K.H.L. Zhang is grateful for funding support from the Herchel Smith Fellowship by University of Cambridge and the Thousand Youth Talents Program of China. We thank Diamond Light Source for access to beamline I09 (SI 16005), which contributed to the results presented here. We also thank beamline scientist Christoph Schlueter at Diamond Light Source for their assistance. This material is based upon work supported by the Air Force Office of Scientific Research under award number FA9550-18-1-0024. This work made use of the UCL Grace and Legion high-performance computing resources and the ARCHER UK National Supercomputing Service (<http://www.archer.ac.uk>), via membership of the UK's HEC Materials Chemistry Consortium, which is funded by the EPSRC (EP/L000202). A.J. Jackson and D.O. Scanlon acknowledge support from the EPSRC (EP/N01572X/1).

* lpiper@binghamton.edu

¹ T. Kamiya and H. Hosono, *NPG Asia Materials* **2**, 15 (2010).
² E. Fortunato, P. Barquinha, and R. Martins, *Advanced Materials* **24**, 2945 (2012), ISSN 1521-4095.
³ X. Yu, T. J. Marks, and A. Facchetti, *Nature Materials* **15**, 383 (2016), ISSN 1476-1122, URL <https://www.nature.com/articles/nmat4599>.
⁴ H. Hosono, *Japanese Journal of Applied Physics* **52**, 090001 (2013).
⁵ H. Kawazoe, M. Yasukawa, H. Hyodo, M. Kurita, H. Yanagi, and H. Hosono, *Nature* **389**, 939 (1997), ISSN 0028-0836.
⁶ H. Yanagi, S.-i. Inoue, K. Ueda, H. Kawazoe, H. Hosono, and N. Hamada, *Journal of Applied Physics* **88**, 4159 (2000), ISSN 00218979, URL <http://scitation.aip.org/content/aip/journal/jap/88/7/10.1063/1.1308103>.
⁷ Y. Ogo, H. Hiramatsu, K. Nomura, H. Yanagi, T. Kamiya, M. Kimura, M. Hirano, and H. Hosono, *Physica Status Solidi (a)* **206**, 2187 (2009), ISSN 18626300.

⁸ M. J. Wahila, K. T. Butler, Z. W. Lebens-Higgins, C. H. Hendon, A. S. Nandur, R. E. Treharne, N. F. Quackenbush, S. Sallis, K. Mason, H. Paik, et al., *Chemistry of Materials* **28**, 4706 (2016), ISSN 0897-4756.
⁹ K. H. L. Zhang, Y. Du, A. Papadogianni, O. Bierwagen, S. Sallis, L. F. J. Piper, M. E. Bowden, V. Shutthanandan, P. V. Sushko, and S. A. Chambers, *Advanced Materials* **27**, 5191 (2015), ISSN 1521-4095.
¹⁰ J. Y. Zhang, W. W. Li, R. L. Z. Hoyer, J. L. MacManus-Driscoll, M. Budde, O. Bierwagen, L. Wang, Y. Du, M. J. Wahila, L. F. J. Piper, et al., *J. Mater. Chem. C* **6**, 2275 (2018), URL <http://dx.doi.org/10.1039/C7TC05331B>.
¹¹ A. Walsh, J. L. F. Da Silva, and S.-H. Wei, *Phys. Rev. Lett.* **100**, 256401 (2008), URL <https://link.aps.org/doi/10.1103/PhysRevLett.100.256401>.
¹² F.-L. Schein, M. Winter, T. Böntgen, H. Von Wenckstern, and M. Grundmann, *Applied Physics Letters* **104**, 2 (2014), ISSN 00036951.
¹³ H. Mizoguchi, M. Hirano, S. Fujitsu, T. Takeuchi, K. Ueda, and H. Hosono, *Applied Physics Letters* **80**, 1207 (2002), ISSN 00036951.

- ¹⁴ D. M. Ramo and P. D. Bristowe, *Journal of Chemical Physics* **141** (2014), ISSN 00219606, URL <http://dx.doi.org/10.1063/1.4893556>.
- ¹⁵ T. R. Paudel, A. Zakutayev, S. Lany, M. D’Avezac, and A. Zunger, *Advanced Functional Materials* **21**, 4493 (2011), ISSN 1616301X.
- ¹⁶ K. Nomura, T. Kamiya, and H. Hosono, *Advanced Materials* **23**, 3431 (2011), ISSN 1521-4095, URL <http://www.ncbi.nlm.nih.gov/pubmed/21721056>.
- ¹⁷ H. J. Kim, I. C. Song, J. H. Sim, H. Kim, D. Kim, Y. E. Ihm, and W. K. Choo, *Journal of Applied Physics* **95**, 7387 (2004), ISSN 00218979.
- ¹⁸ W. Walukiewicz, *Physica B* **303**, 123 (2001).
- ¹⁹ J. Robertson and S. J. Clark, *Physical Review B* **83**, 075205 (2011), ISSN 1098-0121, URL <http://link.aps.org/doi/10.1103/PhysRevB.83.075205>.
- ²⁰ J. Robertson, *Journal of Vacuum Science & Technology A* **31**, 050821 (2013).
- ²¹ A. Walsh and K. T. Butler, *Accounts of Chemical Research* **47**, 364 (2014), ISSN 00014842.
- ²² S. Narushima, H. Mizoguchi, K. I. Shimizu, K. Ueda, H. Ohta, M. Hirano, T. Kamiya, and H. Hosono, *Advanced Materials* **15**, 1409 (2003), ISSN 09359648.
- ²³ K. H. L. Zhang, K. Xi, M. G. Blamire, and R. G. Egdell, *Journal of Physics: Condensed Matter* **28**, 383002 (2016), ISSN 0953-8984.
- ²⁴ N. Mansourian-Hadavi, S. Wansom, N. H. Perry, A. R. Nagaraja, T. O. Mason, L.-h. Ye, and A. J. Freeman, *Phys. Rev. B* **81**, 075112 (2010), URL <https://link.aps.org/doi/10.1103/PhysRevB.81.075112>.
- ²⁵ D. O. Scanlon and G. W. Watson, *Physical chemistry chemical physics : PCCP* **13**, 9667 (2011), ISSN 1463-9084.
- ²⁶ K. Samanta, P. Bhattacharya, R. S. Katiyar, W. Iwamoto, R. R. Urbano, P. G. Pagliuso, and C. Rettori, *Materials Research Society Symposium Proceedings* **891**, 0891 (2006), ISSN 0022-3727.
- ²⁷ T. Kamiya, S. Narushima, H. Mizoguchi, K. Shimizu, K. Ueda, H. Ohta, M. Hirano, and H. Hosono, *Advanced Functional Materials* **15**, 968 (2005), ISSN 1616-301X.
- ²⁸ M. Dekkers, G. Rijnders, and D. H. A. Blank, *Applied Physics Letters* **90**, 1 (2007), ISSN 00036951.
- ²⁹ O. Volnianska and P. Boguslawski, *Journal of Applied Physics* **114** (2013), ISSN 00218979.
- ³⁰ M. N. Amini, H. Dixit, R. Saniz, D. Lamoen, and B. Partoens, *Physical chemistry chemical physics : PCCP* **16**, 2588 (2014), ISSN 1463-9084.
- ³¹ G. Kresse and J. Furthmüller, *Phys. Rev. B* **54**, 11169 (1996), ISSN 0163-1829.
- ³² G. Kresse and J. Furthmüller, *Comput. Mater. Sci.* **6**, 15 (1996), ISSN 09270256, 0927-0256(96)00008, URL <https://www.sciencedirect.com/science/article/pii/0927025696000080>.
- ³³ G. Kresse and D. Joubert, *Phys. Rev. B* **59**, 1758 (1999), ISSN 0163-1829, URL <http://link.aps.org/doi/10.1103/PhysRevB.59.1758>.
- ³⁴ J. P. Perdew, A. Ruzsinszky, G. I. Csonka, O. A. Vydrov, G. E. Scuseria, L. A. Constantin, X. Zhou, and K. Burke, *Phys. Rev. Lett.* **100**, 136406 (2008), ISSN 0031-9007, URL <http://link.aps.org/doi/10.1103/PhysRevLett.100.136406>.
- ³⁵ A. Jain, S. P. Ong, G. Hautier, W. Chen, W. D. Richards, S. Dacek, S. Cholia, D. Gunter, D. Skinner, G. Ceder, et al., *APL Materials* **1**, 011002 (2013), ISSN 2166532X, URL <http://link.aip.org/link/AMPADS/v1/i1/p011002/s1\&Agg=doi>.
- ³⁶ Materials Project Database item mvc-6068, DOI: 10.17188/1321879.
- ³⁷ P. E. Blöchl, O. Jepsen, and O. K. Andersen, *Phys. Rev. B* **49**, 16223 (1994), ISSN 01631829, URL <https://link.aps.org/doi/10.1103/PhysRevB.49.16223>.
- ³⁸ J. Kelly and S. G. Alcock, *Journal of Physics: Conference Series* **425**, 052024 (2013).
- ³⁹ L. W. Wangoh, S. Sallis, K. M. Wiaderek, Y.-C. Lin, B. Wen, N. F. Quackenbush, N. A. Chernova, J. Guo, L. Ma, T. Wu, et al., *Applied Physics Letters* **109**, 053904 (2016).
- ⁴⁰ N. F. Quackenbush, H. Paik, M. J. Wahila, S. Sallis, M. E. Holtz, X. Huang, A. Ganose, B. J. Morgan, D. O. Scanlon, Y. Gu, et al., *Phys. Rev. B* **94**, 085105 (2016), ISSN 1550235X.
- ⁴¹ K. Fleischer, E. Norton, D. Mullarkey, D. Caffrey, and I. V. Shvets, *Materials* **10**, 19 (2017), ISSN 19961944.
- ⁴² J. I. Pankove, *Optical Processes in Semiconductors* (Dover Publications, Inc., 1971), ISBN 9780486602752.
- ⁴³ B. N. Figgis and M. A. Hitchman, *Ligand Field Theory and Its Applications*, Special topics in inorganic chemistry (Wiley-VCH, 2000), ISBN 9780471317760.
- ⁴⁴ R. Drasovean and S. Condurache-Bota, *Journal of Optoelectronics and Advanced Materials* **11**, 2141 (2009), ISSN 1454-4164.
- ⁴⁵ O. Laporte and W. F. Meggers, *J. Opt. Soc. Am.* **11**, 459 (1925).
- ⁴⁶ V. F. Drobný and L. Pulfrey, *Thin Solid Films* **61**, 89 (1979), ISSN 00406090.
- ⁴⁷ E. S. Goh, J. W. Mah, and T. L. Yoon, *Computational Materials Science* **138**, 111 (2017), ISSN 09270256, 1703.02496, URL <http://dx.doi.org/10.1016/j.commatsci.2017.06.032>.
- ⁴⁸ N. F. Quackenbush, J. P. Allen, D. O. Scanlon, S. Sallis, J. a. Hewlett, a. S. Nandur, B. Chen, K. E. Smith, C. Weiland, D. a. Fischer, et al., *Chemistry of Materials* **25**, 3114 (2013), ISSN 0897-4756.
- ⁴⁹ X. Nie, S.-H. Wei, and S. B. Zhang, *Physical Review Letters* **88**, 066405 (2002), ISSN 0031-9007.